InterPore JOURNAL

Original Research

EVOLUTION OF FRICTIONAL STRENGTH OF DRY SHEARED GRANULAR POROUS MEDIA DURING SLIP-RATE WEAKENING

Sahar Bakhshian[1,2], Muhammad Sahimi[1]

[1]Mork Family Department of Chemical Engineering and Materials Science, University of Southern California, Los Angeles, California, USA; [2]Current: Department of Earth, Environmental, and Planetary Sciences, Rice University, Houston, Texas, USA

Correspondence to:
Muhammad Sahimi at moe@usc.edu

How to Cite:
Bakhshian, S., & Sahimi, M. (2024). Evolution of Frictional Strength of Dry Sheared Granular Porous Media During Slip-Rate Weakening. InterPore Journal, 1(2), ipj240824–5. https://doi.org/10.69631/ipj.v1i2nr16

RECEIVED: 26 Nov. 2023
ACCEPTED: 6 Aug. 2024
PUBLISHED: 24 Aug. 2024

ABSTRACT

Using the discrete-element method, we study loss of shear strength at frictional asperity contacts, induced by flash heating, in a granular fault gouge. The magnitude of the reduction in the shear stress and the local friction coefficients are computed over a wide range of shear velocities V_s. For small strain rates, there is negligible difference between the frictional stress for packings with and without frictional weakening that arises due to flash heating. As strain rate increases, however, the difference between the two becomes significant. The results indicate a clear transition in the shear stress-shear strain response corresponding to $V_s > 0.3$ m/s and those with $V_s \leq 0.3$ m/s. Specifically, the stress–strain diagrams at lower V_s exhibit a pronounced decreasing strength over small distances, whereas they indicate a progressive increase in the shear stress at higher V_s, which is reminiscent of a transition from ductile behavior at high velocities to brittle response at low velocities. Only a small fraction of the contacts experience lower friction, with the majority having friction coefficients closer to 0.5, hence suggesting that fast slip is accommodated only at a few contacts, with the rest either not sliding at all, or sliding very slowly. Moreover, if we define an effective macroscopic friction coefficient, $\mu e = \tau/P$, where τ is the shear stress, and P is the pressure, and the inertial number I by, $I = \gamma D\sqrt{\rho/P}$, where γ is the strain rate, and D is the average size of the particles, we find that the weakening packing follows a nonlinear friction law, well approximated by, $\mu e \approx I^{3/4}$. Thus, the model with flash heating deviates from linear friction law even at smaller, albeit not too small, values of I, which is intriguing and novel. The implications of the results for earthquake physics and the principal slip planes in fault z ones are discussed.

KEYWORDS

Granular porous media, Frictional strength, Slip-rate weakening, Flash heating

@2024 The Authors
This is an open access article published by InterPore under the terms of the Creative Commons Attribution-NonCommercial-NoDerivatives 4.0 International License (CC BY-NC-ND 4.0) (https://creativecommons.org/licenses/by-nc-nd/4.0/).

1. INTRODUCTION

An important factor that controls earthquake rupture propagation and the ensuing seismic instability is the dynamic friction of faults (5, 43). Previous studies attempted to demonstrate reduction of fault friction and its strength during earthquakes with high slip rates (23), a process known as slip-rate weakening (19, 47). Thus, the general thinking is that strain softening (frictional weakening) triggers the seismic instability, leading to earthquakes, and that a fault weakens with increasing slip rates (40, 44), which also affects the magnitude of earthquakes (10).

It has been reported that the weakening phenomenon during fault slip may be activated by thermal pressurization of pore fluids and flash heating (5, 11, 24, 26, 32, 45), a microscopic phenomenon in which heat is generated at asperity contacts due to high shear slip rates, i.e., fast fault motion. Because the thermal conductivity of rock and gouge is low, the heat generated at the contact points or surfaces cannot diffuse fast enough, as a result of which heat is accumulated at the contacts, increasing the local contact temperature and reducing its frictional shear strength. Rice (40, 41) developed a theory of flash heating at frictional asperity contacts to describe the weakening behavior and the dependence of fault friction on the slip rate in rocks. Note, however, that flash heating can, in principle, occur not only at asperities but also on smooth surfaces. The only requirement is the supply of sufficient heat over a short period of time so that the temperature may spike, and then cool down quickly. Thus, with two smooth surfaces sheared at high stress and slip rate over a brief period of time, flash heating may occur.

Experimental studies on rock and gouge friction under high slip rates indicate the presence of frictional weakening for slip rates larger than 0.3 m/s, independent of rock or gouge type, which is attributed mainly to flash heating (11). For example, an experimental study of quartz rocks (18) revealed that, due to rock weakening at sub-seismic slip rates, the friction coefficient decreases by a factor of 3. O'Hara et al. (36) demonstrated weakening response of the coal gouge as a result of frictional heating at high slip rates, which was approximately 1 m/s. These data indicate the presence of various phenomena during slip experiments, including frictional heating, fluid pressurization, thermal decomposition, and silica gel formation (40).

Using a theory of shear-transformation zone (STZ), Elbanna and Carlson (12) proposed a model for flash weakening in granular porous media to study their shear behavior under various sliding rates and confining pressures. Their model predicted a logarithmic dependence of steady-state shear strength on the imposed slip velocity at low slip rates, but strong rate-weakening response at high slip rates. A velocity-weakening friction model based on the flash heating concepts was developed by Lucas et al. (28) that accurately predicted the friction coefficient of landslides on Earth, and reported a reduction of friction coefficient with increasing sliding velocity. In a previous paper (38), we employed molecular dynamics (MD) simulations—the first such use, to our knowledge—to study sliding friction between two SiO_2 (quartz) surfaces (common in sandstones). We computed the temperature profile within the system, focusing on the interface between the surfaces, and examined the temperature dependence of thermal conductivity in both crystalline and amorphous SiO2. Additionally, we analyzed the effects of slab thickness on heat transfer to simulate and understand flash heating.

Our MD simulations indicated that as the interfacial temperature increases, bonds between the atoms begin to break, resulting in molecular-scale fracture that eventually produces the flash heating. Increasing the sliding velocity also increases the frequency of flash heating events, which leaves increasingly shorter times for the material to relax. As a result, interfacial temperature increases. If the sliding slabs are thin, the heat quickly diffuses away from the interface, sharply decreasing the temperature immediately after flash heating. But with increasing thickness, as in real rock, the rate of heat transfer is reduced significantly, which keeps most of the heat close to the interface and produces

weakened material. The weakening behavior was demonstrated by computing the stress–strain diagrams, which indicated that, for small strain rates, the frictional stress is essentially independent of the materials' thickness. As the strain rate increases, however, the dependence becomes stronger. Specifically, the stress–strain diagrams at lower velocities exhibit a pronounced decreases in the strength over small distances, whereas they exhibit progressive increase in the shear stress at higher velocities.

The present paper represents a continuum-scale version of our previous study. To gain a deeper understanding of frictional weakening, as well as checking whether the results with a continuum-scale model agree with those obtained by MD simulations, we have carried out extensive computer simulation of slip in granular porous media over a range of slip rates, from 0.05 m/s to 1 m/s, and have assessed their shear response to sliding velocity V_s as its magnitude was varied. Variation of the local friction coefficient and the dynamic evolution of the frictional strength induced by slip-rate weakening have also been investigated.

We should point out that, since our original MD simulations described above, Mollon et al. (33) and Taboada and Renouf (46) reported studies of the same phenomenon in two-dimensional (2D) models. Mollon et al. (33) utilized the standard discrete element method (DEM) of Cundall and Strack (6). Taboada and Renouf (46) also used the same 2D model, and introduced a temperature-dependent friction coefficient through an empirical equation, although the friction coefficient depends on the weakening velocity. Their results are in qualitative agreement with ours reported in the present paper for a 3D model (see below).

The rest of this paper is organized as follows. In the next section, the model and the details of computer simulation are described. In **Section 3** the results are presented, and their implications are discussed. The paper is summarized in the last section.

2. MATERIALS AND METHODS: COMPUTER SIMULATION PROCEDURE

We used the 3D DEM of Potyondy and Cundall (39), which represents an updated and refined version of the original model of Cundall and Strack (6), to carry out computer simulation of the phenomenon in a 3D packing of spherical particles.

2.1. The Model

Over very small time steps, the disturbances caused by an external force propagates from any particle to only its immediate neighbors. Thus, in the DEM, only the pair-wise interaction between the neighboring particles is considered. Due the high computational cost, the DEM is implemented in a parallel scheme using OpenMP (8). The evolution of the packing under shear is simulated by solving Newton's law of motion. We used a modification of the Verlet algorithm (16, 27), the half-step leapfrog Verlet algorithm, in which the velocity is first calculated at each half time step, i.e., at $(t + \Delta t/2)$, then the position $x(t + \Delta t)$ is computed, and finally the velocity at time $(t + \Delta t)$ is calculated, where Δt is the size of the time step. The translational and rotational motion of each particle is governed by: **Equation 1** and **Equation 2** where m_i, v_i, r_i, I_i, and w_i are, respectively, the mass, linear velocity, radius, moment of inertia, and angular velocity of particle i, while g is the gravitational constant, and superscripts n and t refer to the force's normal and tangential components.

$$m_i \frac{dv_i}{dt} = m_i g + \sum_j \left(F_{ij}^n + F_{ij}^t\right) \tag{1}$$

$$I_i \frac{d\omega_i}{dt} = \sum_j r_i \times F_{ij}^t \tag{2}$$

The normal overlap between two particles for each contact was calculated by **Equation 3** where R_i and x_i are, respectively, the radius of particle i, and its position vector.

$$\delta_n = R_i + R_j \, |x_i \quad x_j| \tag{3}$$

After detecting the contact overlaps, the normal and tangential contact forces, F^n and F^t, are computed using the Hertzian contact model (**Equation 4**, **Equation 5**).

$$F^n = -k_n \delta_n^{3/2} \tag{4}$$

$$F^t = k_t \delta_t \tag{5}$$

Here, k_n and k_t are the normal and tangential stiffness, and δ_t is the cumulative tangential shear displacement. k_n is given by **Equation 6** (39):

$$k_n = 4RY \tag{6}$$

with Y being the effective Young's modulus, and R the equivalent radius of the contacting particles, which, for contacting particles i and j, are given by **Equation 7** and **Equation 8**:

$$R = \left(\frac{1}{R_i} + \frac{1}{R_j}\right)^{-1} \tag{7}$$

$$Y = \left(\frac{1 \quad {v_i}^2}{Y_i} + \frac{1 \quad {v_j}^2}{Y_j}\right)^{-1} \tag{8}$$

with ν being the Poisson's ratio. Using **Equation 9**, δ_t is calculated incrementally by integrating the tangential component of the relative velocity at the contact point:

$$\delta_t = \int v_t dt \tag{9}$$

where v_t is the tangential contact velocity, defined by **Equation 10**.

$$v_t = (v_i \quad v_j)t + \omega_i R_i + \omega_j R_j \tag{10}$$

Here, t is the tangential component of the unit vector connecting the contacting particles' centers, and ω_i is the angular velocity of particle i. According to Coulomb's law of friction, $F^t \leq \mu_s |F^n|$, where μ_s is the static friction coefficient. Sliding occurs at the contact points when the tangential force exceeds the static friction. The time step Δt must be small enough to maintain the assumption of constant translational and rotationl accelerations, and to carry out numerically stable simulation. The number of time steps N is estimated by (13), $N \sim \sqrt{Y}/(\rho \bar{R})$, where $\bar{R}$ denotes the average radius of the particles, with ρ being their density.

2.2. Friction Model of Weakening due to Flash Heating

Suppose that T_a is the average temperature of the fault surface. As sliding occurs and asperity contact forms, flash heating causes temperature at the asperity contact to increase for a high-speed sliding. Then, as the contact slides, its temperature rises during its brief lifetime, $\theta = D_a/V_s$, where $D_a = 2R$ is the contact diameter, and V_s is the shear velocity or slip rate. The temperature increase is essentially due to the generated heat localized at the asperity contact at a rate of $\tau_c V_s$, where τ_c is the frictional strength of the asperity contact, which we assume to be nearly constant. But, when $T_a > T_w$, where T_w is the weakening temperature, the frictional strength of the asperity contact decreases to a weakened value $\tau_w \ll \tau_c$. For a large V_s, the generated heat at the asperity interface does not have sufficient time to propagate quickly, and the contact point attains the weakened temperature T_w over a time $\theta_w < \theta$. Following Rice (40, 41), we assume 1D heat conduction at the asperity contact, so that from the solution of the governing heat conduction equation, θ_w is obtained using **Equation 11**:

$$\theta_w = \frac{\pi \alpha}{V_s^2}\left[\frac{\rho c (T_w \quad T)}{\tau_c}\right]^2 \tag{11}$$

where α is the thermal diffusivity, and ρ_c is the total heat capacity (per volume). Thus, the critical weakening velocity $V_w = D_a/\theta_w$ is given by **Equation 12**:

$$V_w = \frac{\pi\alpha}{D_a}\left[\frac{\rho c(T_w \quad T)}{\tau_c}\right]^2 \tag{12}$$

Note that we assumed that the contact diameter is $D_a = 2R$. One can show that $D_a \propto R^{1/3} < R$. Despite this, substituting for the various parameters in **Equation 12**, we obtain $V_w \approx 0.3\ m/s$, consistent with the theoretical estimate of Rice (40, 41) and experimental data of Beeler et al. (2), so that the assumption is reasonably accurate, and, at the same time, there is nothing in **Equation 12** that prevents one from using a smaller contact diameter. Thus, for velocities greater than V_w, the weakening occurs at the asperity contacts, whereas for those smaller than V_w, there is no weakening, implying that for $V_s < V_w$, the contacts are strong enough during their entire lifetime. But, when $V_s > V_w$, i.e., when $\theta_w < \theta$, the contacts spend a fraction V_w/V_s of their lifetime with high strength, while the remaining fraction is in the weakened state. By ignoring the statistical distribution of contact diameters D_a (whose effect is of second order), the weakened friction coefficient μ_w of the fault is given by (28, 40) (**Eq. 13**):

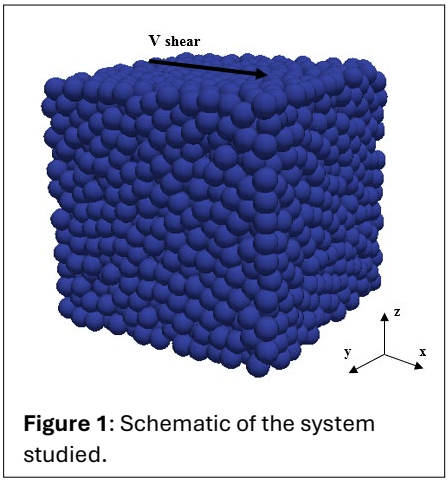


Figure 1: Schematic of the system studied.

$$\mu_w = \begin{cases} \mu_s & V_s \le V_w \\ \dfrac{\mu_s}{1 + V_s/V_w} & V_s > V_w \end{cases} \tag{13}$$

For typical values of the thermal diffusivity α in crustal rocks, one expects (40) the increase in the temperature to be localized at the asperity contacts. More precisely, over the contact lifetime t_c, the heat diffuses a distance of approximately $(\alpha t_c)^{1/2}$. For a contact size of few microns, and $V_s = 1\ m/s$, the contact time is approximately 10^{-5} s. Thus, with $\alpha \approx 5 \times 10^{-7}\ m^2/s$, the distance over which the heat diffuses would be around $10^{-6} m$, which is very small compared with the particles' diameter. It is therefore justified to assume that all the heat remains localized in the contact plane, and that the resulting shear heating has an instantaneous effect on the local friction coefficient. Thus, we incorporated the flash weakening theory, **Equations 11** to **13**, in the shear simulations.

Table 1: Micromechanical and geometrical properties of the packing.

Parameter	Value	Units
Number of Particles	3000	
Particle Radius $\boldsymbol{R}$	3	mm
Domain Dimensions	86 × 86 × 85	mm^3
Particle Density $\boldsymbol{\rho}$	2.650	$gr.cm^3$
Normal Stiffness $\boldsymbol{k_n}$	3.247×10^3	$N.mm^{-1}$
Tangential Stiffness $\boldsymbol{k_t}$	3.247×10^3	$N.mm^{-1}$
Poisson's Ratio $\boldsymbol{v}$	0.26	
Young's Modulus $\boldsymbol{Y}$	0.69	GPa
Shear Modulus $\boldsymbol{Y_s}$	0.273	GPa
Static Friction Coefficient $\boldsymbol{\mu_s}$	0.5	
Normal Stress $\boldsymbol{\sigma_n}$	10	MPa
Time Step $\boldsymbol{\Delta t}$	0.005	μs
Thermal Diffusivity $\boldsymbol{\alpha}$	0.5	$Mm^2.s^{-1}$
Volumetric Heat Capacity $\boldsymbol{\rho c}$	2.7	MPa/°C
Weakening Temperature $\boldsymbol{T_w}$	1000	°C
Average Temperature $\boldsymbol{T_a}$	400	°C
Frictional Strength $\boldsymbol{\tau_c}$	45	MPa

The granular packing was generated using the method described previously (1). After some preliminary simulations for identifying a suitable size of the packing, a large packing with several thousand particles was constructed. As the preshear process, the packing was compressed by applying a normal stress σ_n to its top dynamic boundary, after which the shear test was implemented by moving the top layer of the particles at a constant horizontal

velocity V_s, as shown in **Figure 1**, while the lower boundary was held fixed. To keep the packing normally compressed, the upper stress boundary condition must be satisfied during the shearing simulations. Shear simulations were carried out at a confining stress of 10 MPa, with periodic boundary conditions utilized in the x and y directions.

Two cases were simulated. (i) The no-weakening packing in which the local friction coefficient between the particles was constant, $\mu_s = 0.5$. (ii) The weakening packing in which the local friction coefficient was varied according to **Equation 13**. The frictional strength of the asperity contact τ_c was taken to be 1/6 of the shear modulus Y_s. The results of the simulations were analyzed over the time scale that spanned from $t = 0$ until steady state was reached.

The input parameters for the simulation, taken from Rice (40), are listed in **Table 1**. We simulated the system for shear velocities V_s = 0.05, 0.08, 0.1, 0.2, 0.5 and 1 m/s. We note that the size of the particle is larger than those of a fault gouge, which is typically on the order of 1^{-10} μm (42). While this might seemingly imply that the assumption that the heat generated at the contacts can only diffuse a small distance relative to the size of the grain, is questionable, the very low conductivity of rock materials, which we computed by our MD simulations, indicates that the assumption is valid.

In addition, the question of the effect of the size of the particles can be addressed by assuming a distribution of local friction coefficients, rather than a single value. However, past experience in many contexts has indicated that, so long as the distribution is not pathological and has no unusual features (such as, for example, divergent higher moments), an average value of the distribution should be adequate.

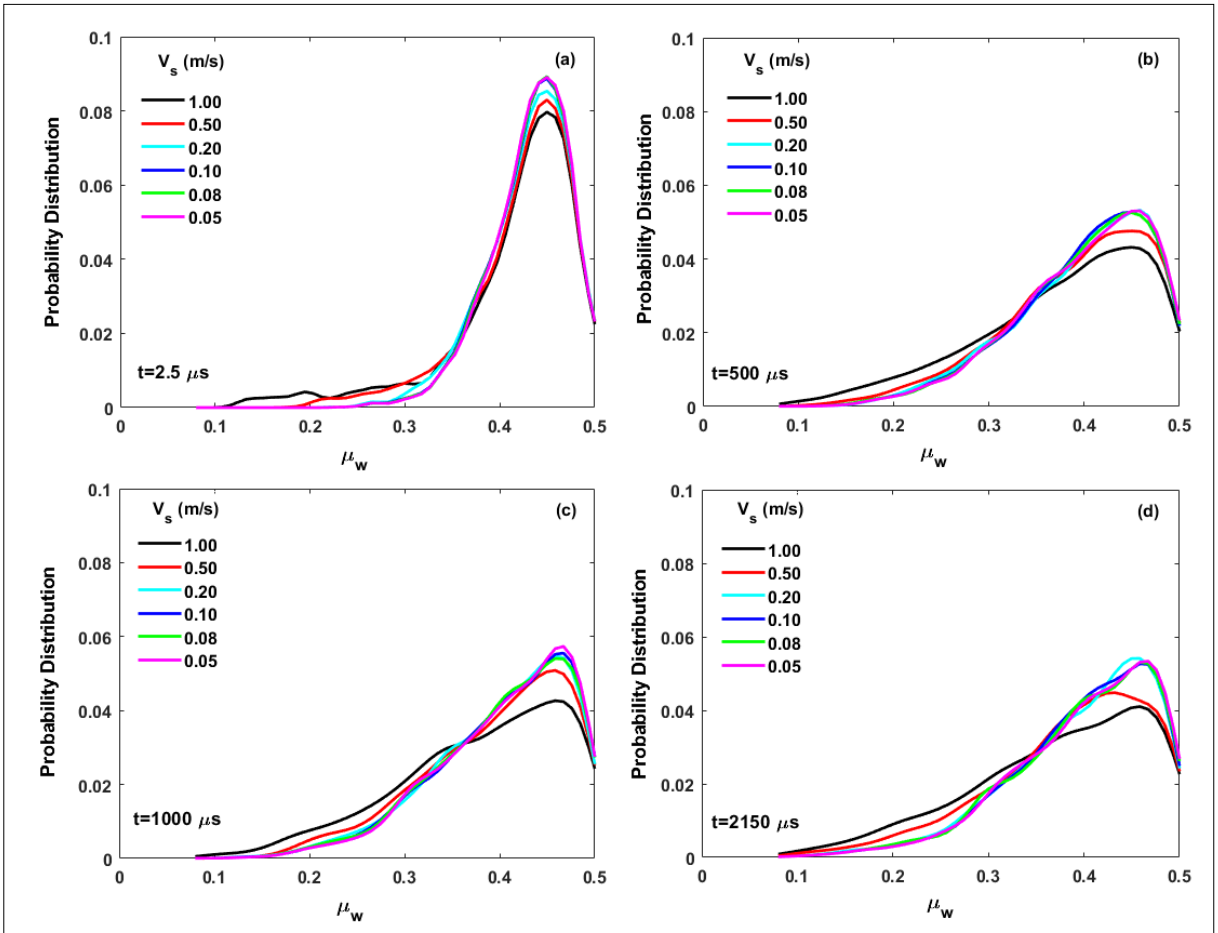


Figure 2: Probability distribution function of the weakened friction coefficient μ_w for various shear velocities (V_s) at times (all in μs) **(a)** 2.5; **(b)** 500; **(c)** 1000; and **(d)** 2150.

To guarantee the stability and accuracy of the results in the absence of damping, one must determine the size of the time that emerges from the translational and rotational degrees of freedom and the sonic wave velocity (37). The time step given in **Table 1** was selected based on such considerations.

3. RESULTS

The histograms of the weakened local friction coefficient μ_w are shown in **Figure 2**, representing their distributions over the shear test time. **Figure 2a** indicates that, within the initial microseconds and for all the sliding rates V_s, a small percentage of the particles experience weakening as μ_w is mostly between 0.3 and 0.5. For higher V_s, the decrease in μ_w is even higher. At longer times, the distribution of μ_w has a longer tail of smaller values, indicating that over such times the weakening state is more widely spread, penetrating more deeply into the packing. **Figure 2** also indicates that since only a small fraction of the contacts experience lower friction, with most of them having a μ_w closer to 0.5, fast slip is accommodated only at a few contacts, while most of the other contacts are either not sliding at all, or sliding slowly. This is consistent, at least qualitatively, with the aforementioned STZ theory (14, 15, 29, 30) that suggests that non-affine deformation is localized in a small number of spots that are continuously created and annihilated.

Figure 3 presents the velocity profiles in the weakening packing. Each point represents an average over the xy plane. At high V_s the velocity profiles are smooth. This may be explained by considering **Equation 13**. A relatively large V_s corresponds to a low friction coefficient μ_w. For low V_s, the friction coefficients for some of the particles increase, while it remains the same for others, hence giving rise to fluctuations in the local velocities of the particles.

Our simulations indicate that small sliding velocities lead to lower overall friction but larger stress drops, whereas for high velocities frictional strengthening takes place in which the value of friction depends on the shearing velocity. It may appear that such a frictional strengthening is surprising, but experiments by

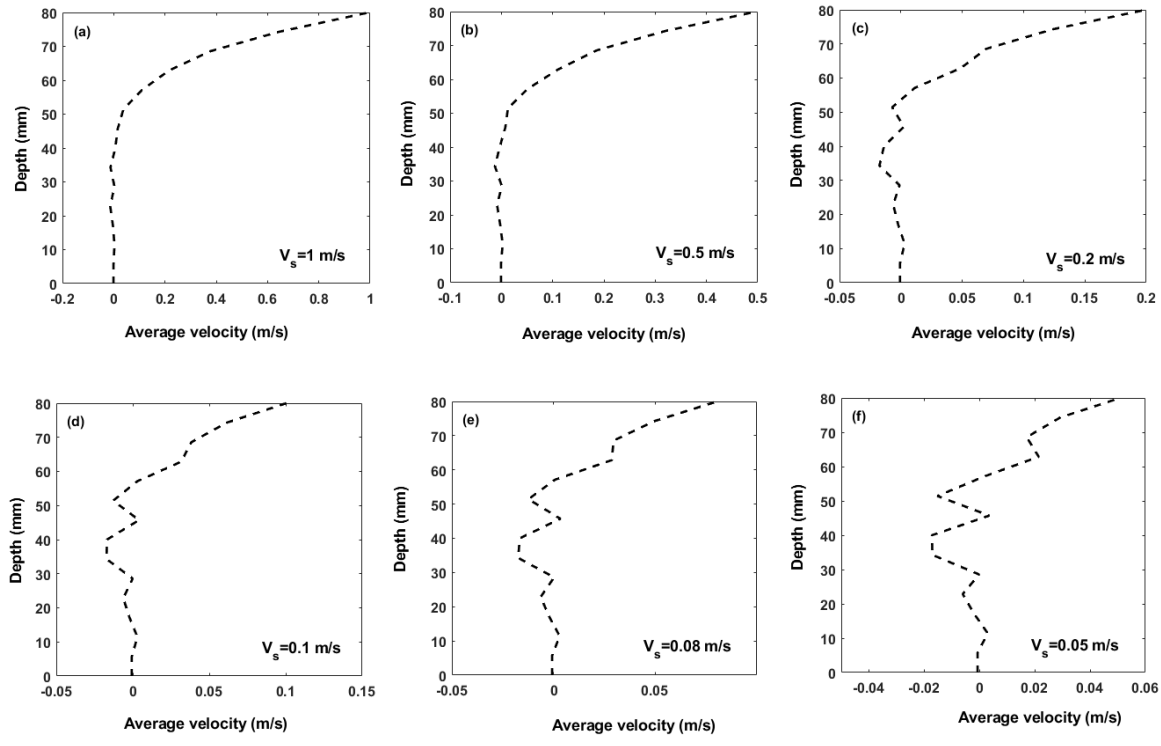


Figure 3: The velocity profiles and their dependence on the depth, measured from the bottom of the packing, with the average taken over the xy plane (see **Fig. 1**).

Ikari et al. (20) actually support this. Studying natural fault gouge samples from the Waikukupa Thrust in southern New Zealand, Ikari et al. (20) showed that in the early stages of loading following a slip event, there is a period of increased stability, which gradually disappears as slip accumulates. Thus, in terms of rate- and state-dependent friction laws, the frictional strengthening and temporary stable phase of the system exist as long as slip is less than a critical slip distance and time is less than the value of the state variable at steady state.

Figure 4 summarizes these findings. **Figure 4a** presents the shear stress-shear strain diagram associated with V_s = 1 m/s, indicating that there is negligible difference between the frictional stresses of the two packings for small strains. As strain increases, however, the difference between the two becomes more significant, until they reach the steady state and their differences remain almost unchanged. The steady shear stress for the non-weakening packing is around 0.22 GPa, whereas for the weakening case, it is approximately 0.15 GPa, which is a decrease of circa 32% with thermal weakening.

The results for V_s = 0.5 m/s are depicted in **Figure 4b**. With flash heating, the steady shear stress decreases from 0.11 GPa to 0.09 GPa, an 18% decline. For V_s = 0.2 m/s, the difference between steady shear stress of the two packings reduces (see **Fig. 4c**). The results for a smaller V_s, as shown in **Figure 4d,e** and **f**, indicate that the shear responses of the weakening and non-weakening packings are essentially identical, and that the steady-state shear strength remains almost unchanged, even when there is flash heating. Thus, for $V_s > 0.3$ m/s, the weakening effect is significant, which is in line with the previous studies (11) and, therefore, the effect of thermal weakening at macroscale is more prominent. It is also clear that as the sliding velocity decreases, the shear stress attains the steady-state limit faster.

Figure 4 also indicates a clear transition in the shear stress-shear strain response between the results for $V_s > 0.3$ m/s and those for $V_s \leq 0.3$ m/s. More specifically, the strain-dependence of the stress at lower V_s exhibits a pronounced strength drop over small strains, whereas the results at higher V_s exhibit a progressive increase in the shear stress as a function of the slip. This is reminiscent of the transition between ductile behavior at high velocities to brittle response at low speeds (3, 31, 48). The transition may be a function of the thickness of the deforming medium, which will then bridge the strong rate-weakening effects in bare rock surfaces to diminished rate-weakening effects in gouges in the absence

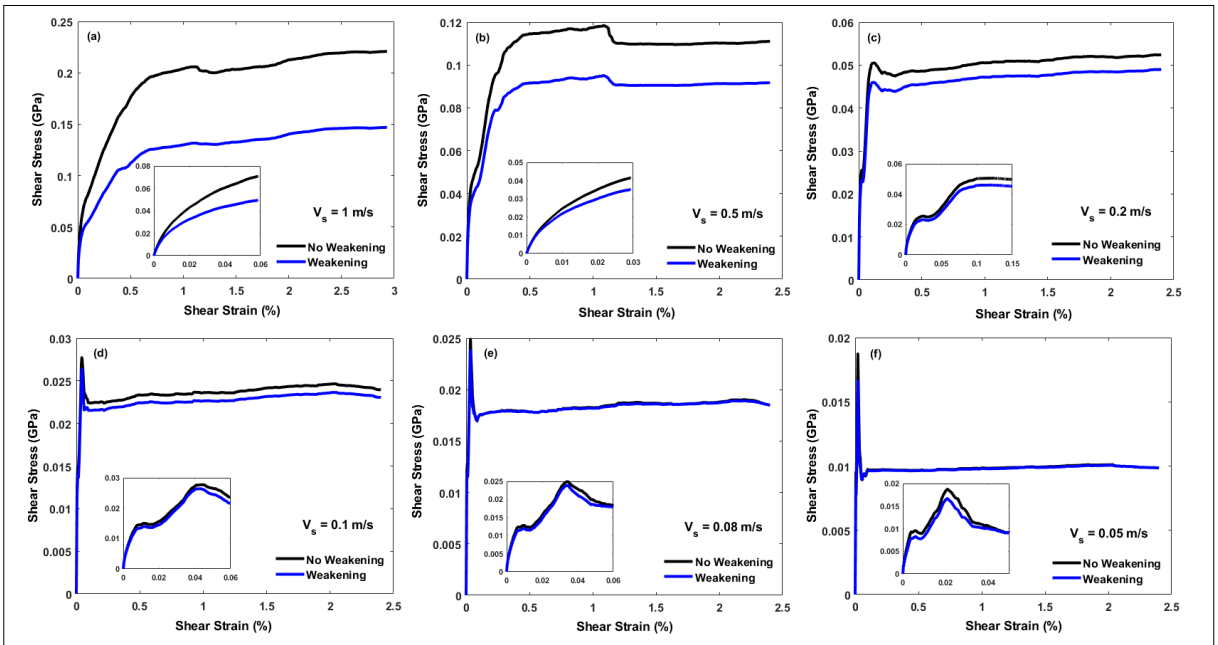


Figure 4: Shear stress-shear strain rate diagrams for constant (no weakening) and variable (weakening) friction coefficients and various shear velocities.

of localized deformation, i.e., thick gouge layers where the slip rate is distributed across the thickness and is not necessarily localized in a plane as in rock surfaces.

The reduction in the shear stress, when the thermal weakening of local friction coefficient is accounted for, is consistent with the predictions of the flash heating theory that the reduction is higher for larger V_s. Note that although thermal weakening is incorporated in the calculation of the shear stress with V_s = 1 m/s, it is still higher than the shear stress with V_s = 0.5 m/s. The expectation is that, with the strong rate-weakening mechanism, the packing becomes weaker as V_s increases. Although this is strictly true for sliding on bare rock surfaces, our results indicate that it does not hold for gouges. The reason may be that granular porous media or gouge exhibit intrinsic rate-strengthening response at high velocities, i.e., the macroscopic shear increases with velocity when its value is high, which competes with the thermal mechanism that favors rate weakening. The competition may be a function of the thickness of the gouge layer. Thermally induced weakening may be more pronounced in thinner layers, or where there is localized deformation similar to sliding on bare rock surfaces. Thicker layers with distributed deformation are governed by rate-strengthening effects.

One may argue that **Figure 4** simply shows the known results for the transient behavior of an elastic response for small shear rates to a plastic response, and that the decrease in the stress is the same as what is usually regarded as a yielding process. That is, if the particles are soft, which may be thought of as corresponding to small shear rates, the elastic response will consist of two parts, namely, the linear response akin to Hookean systems, and a nonlinear response. What **Figure 4** presents goes, however, beyond such results, because it demonstrates that the steady-state shear stress decreases in the case in which we account for the reduction in the strength of local frictional contacts. In other words, in our simulations, the contact friction evolves dynamically, so that weakening/strengthening is dynamic, not prescribed. Previous works, which considered various values of constant local friction coefficient, had suggested that macroscopic friction is in all cases identical, except for the case of frictionless particles. Our simulations highlight the importance of considering the dynamic evolution of the local μ_w, and the fact that such an unsteady process may lead to feedback mechanisms that influence the macroscopic response differently. **Figure 4** also indicates that the simulations have not reached the hard core limit in which the shear rate-dependence disappears. Thus, the results in **Figure 4** may carry a signature from the finite compliance of the particles. It also suggests, however, an inertial effect that seems to initiate sooner in granular porous media with thermal weakening.

Let us define the inertial number I by, $I = \gamma D\sqrt{\rho/P}$, where γ is the strain rate, P is the pressure, and D is the average size of the particles. One may write, $I = t_c/t_s$, where $t_c = d\sqrt{\rho/p}$ is the inertial or confinement time scale, and $t_d = 1/\gamma$ is the shear deformation time scale, both at the grain level. A small I represents the quasistatic critical state regime, whereas a large I corresponds to the collisional regime, which is usually described by the kinetic theory. As we discuss below, the macroscopic inertial number in our simulations is on the order of 10^{-4}, although it is presumably higher locally at the grain scale. Note, however, that even in the hard-core limit at a high I, the rate-dependence persists, a feature that has been documented extensively in the literature (7). If, however, we were to probe much lower values of I, then, the rate-dependence would disappear and would be visible only if we represent the horizontal axis by a logarithmic scale (25).

The existence of a peak in **Figure 4** is generally associated with the variation of the volume fraction of the sample, i.e., dilatancy. Indeed, **Figure 5** presents the dilatancy, defined as $\Delta h/h_0$, where Δh is the change in the weakened packing's height, and h_0 is its initial height. There is significant dilatancy with increasing strain rate $\gamma \leq 0.5\%$, beyond which the dilatancy does not increase any more. Note that according to **Figure 4**, for the packings with $V_s = 0.05 \text{ and } 0.08$ m/s, a shear strain of about 0.5% is the point at which the shear stress becomes independent of the shear strain.

The dependence of the steady shear stress on V_s is an important characteristic of the packings that we study. Our simulations indicate that, at low V_s, there is no difference between the two packings, but once

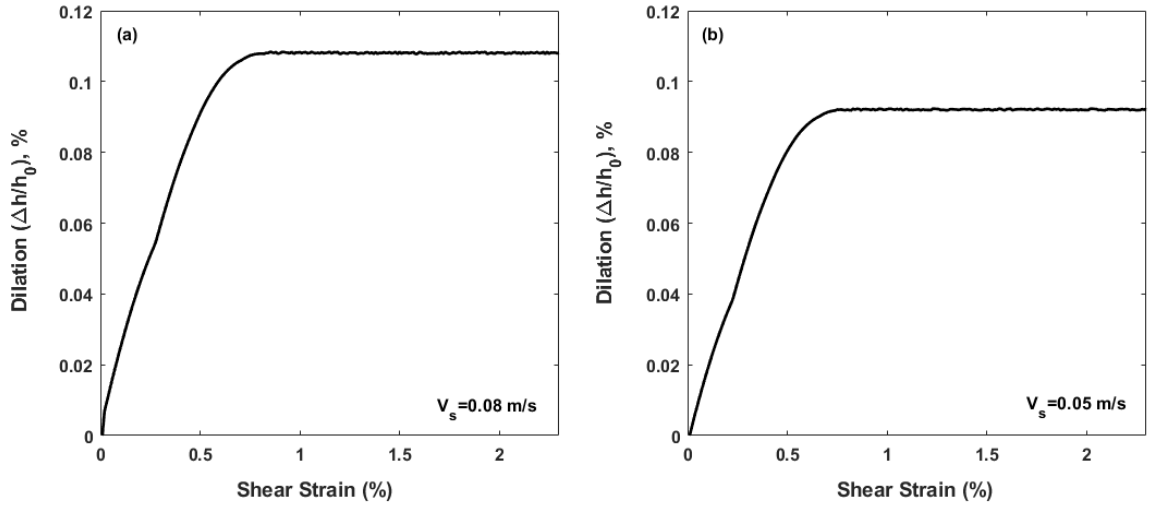


Figure 6: Dependence of dilatancy $\Delta h/h_0$ of the weakening packing on shear strain rate.

$V_s > 0.2$ m/s, the effect of thermal weakening becomes pronounced, and the increase in the shear stress slows down, since the local friction coefficient decreases at such velocities. To demonstrate this, we define an effective friction coefficient μ_e by (17, 31), $\mu_e = \tau/P$, where τ is the shear stress. **Figure 6** presents the computed dependence of μ_e on the inertial number I, which is usually referred to as the *friction law* (17). For the non-weakening packing, the friction law is linear and is represented by, $\mu_e \approx 0.2 + 1.92 \times 10^4 I$, which has been reported by others as well (4, 9, 17, 34). But, the weakening packing follows a nonlinear friction law, which is well approximated by, $\mu_e \approx I^{3/4}$. That our model with flash heating deviates from linear friction law even at smaller, albeit not too small, values of I is intriguing and novel. In addition, the nonlinear response manifested by **Figure 6** presumably indicates that with flash heating the local inertial numbers are higher in the weakening packing, because the contact weakening may promote higher local slip rates and, hence, fluidize the packing locally, thus allowing for a softening response. In principle, a nonlinear friction law is such that as I becomes large, $\mu_e \to \mu_\infty$, which experimental and simulation studies (17, 21, 22) have indicated, but because our simulations do not include large I, such a saturation regime has not emerged yet.

Thus, **Figure 6** suggests that granular porous media with flash heating behave completely differently from those without it, and that the possibility that the nonlinear friction law could be due to the specifics of the packing's preparation, or that the packing may not have been equilibrated, is ruled out because in that case one should have obtained the same behavior even without flash heating. **Figure 6** also suggests that flash heating may not be as effective in granular porous media as it is in sliding on bare rock surfaces. This is due to the competition between the dilatant rate-strengthening characteristics of inertial granular flow, on the one hand, and rate-weakening due to local shear heating, on the other hand. For thicknesses that we have considered in this study, the steady-state shear

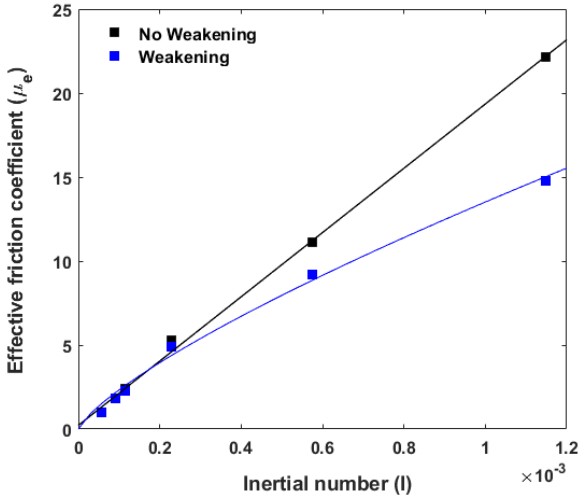


Figure 5: Comparison of the dependence of the effective friction coefficient μ_e on the inertial number I for the weakening and no-weakening packings.

strength increases with increasing slip rate in the absence of localization, although at a lower slope than the cases in which there is no flash heating.

A long standing question in earthquake physics has been why principal slip planes in fault zones are so thin (35). It has been suggested that the thinness may be due to the fact that seismic velocities are high. **Figure 1** provides evidence for this hypothesis. It indicates that the deformation is localized at the top of the granular packing for the velocity of 1 m/s. At lower velocities, however, the deformation is distributed over somewhat larger depths (1). Thus, we may conclude that at higher velocities the deformation is more localized, hence contributing to addressing the dilemma.

4. SUMMARY

Inspired by flash weakening process during earthquakes, we utilized the discrete-element model to study shearing of a granular gouge. The theory of flash heating was incorporated into the DEM simulations in order to study the variations of the local friction coefficient between the particles, as well the evolution of frictional strength, induced by slip-rate weakening. We showed that at relatively high velocities the effect of frictional weakening on the frictional strength of the medium is nontrivial. As strain increases, the difference between the two becomes more significant however, and a clear transition in the shear stress-shear strain diagram emerges when $V_s > 0.3$ m/s to those at ≤ 0.1 m/s. The stress-strain diagrams at lower slip rates exhibit a pronounced strength decrease over small distances, but at higher velocities they exhibit a progressive increase in the shear stress as a function of slip. The simulations also indicate that only a small fraction of the contacts experience lower friction, with most of them having friction coefficients closer to 0.5, hence suggesting that fast slip is accommodated only at few contacts, while most of the other contacts are either not sliding at all, or sliding slowly.

As **Figure 6** suggests, flash heating may not be as effective in thick granular materials as it is in sliding on bare rock surfaces, because the competition between the dilatant rate-strengthening of inertial granular flow, and rate-weakening caused by local shear heating makes flash heating less effective in the granular packings that we studied. If there is no localization and the thickness of a granular packing is on the order of what we considered in this study, the steady-state shear strength increases with increasing slip rate, albeit at a lower slope than when there is no flash heating. Our results also suggest that flash heating alone may not promote strong coherent localization in sheared granular materials and, therefore, other mechanisms, such as thermal pressurization of pore fluids and/or grain interlocking, should also contribute. Thus, the results provide new insights into dynamic weakening mechanisms in fault gouge and the role of flash heating in such systems.

STATEMENTS AND DECLARATIONS

Acknowledgements

This work was supported in part by the Center for Geologic Storage of CO_2, an Energy Frontier Research Center funded by the U.S. Department of Energy (DOE), Office of Science, Basic Energy Sciences (BES), under Award number DE-SC0C12504, by the Petroleum Research Fund, administered by the American Chemical Society, and by grant CBET 2000966 from the National Science Foundation. We acknowledge very useful discussions with Dr. Ahmed Elbanna of the University of Illinois, who first told us about the problem of flash heating, and made many useful suggestions on the initial draft of the manuscript.

Author Contributions

M.S. conceived the problem, acquired funding, provided guidance, and wrote the manuscript. S.B. carried out the numerical simulations. Both authors contributed to interpreting the results.

Conflicts of Interest

The authors have no conflict of interest to declare.

Data, Code & Protocol Availability

Although we used publicly available simulators, they can be obtained from the first author, S.B.

ORCID IDs

Sahar Bakhshian https://orcid.org/0000- 0003-0280-2982
Muhammad Sahimi https://orcid.org/0000-0002-8009-542X

REFERENCES

1. Bakhshian, S., & Sahimi, M. (2016). Computer simulation of the effect of deformation on the morphology and flow properties of porous media. *Physical Review E*, 94(4), 042903. https://doi.org/10.1103/PhysRevE.94.042903
2. Beeler, N. M., Tullis, T. E., & Goldsby, D. L. (2008). Constitutive relationships and physical basis of fault strength due to flash heating. *Journal of Geophysical Research: Solid Earth*, 113(B1), 2007JB004988. https://doi.org/10.1029/2007JB004988
3. Byerlee, J. D. (1968). Brittle-ductile transition in rocks. *Journal of Geophysical Research*, 73(14), 4741–4750. https://doi.org/10.1029/JB073i014p04741
4. Campbell, C. S., Cleary, P. W., & Hopkins, M. (1995). Large-scale landslide simulations: Global deformation, velocities and basal friction. *Journal of Geophysical Research: Solid Earth*, 100(B5), 8267–8283. https://doi.org/10.1029/94JB00937
5. Collettini, C., Viti, C., Tesei, T., & Mollo, S. (2013). Thermal decomposition along natural carbonate faults during earthquakes. *Geology*, 41(8), 927–930. https://doi.org/10.1130/G34421.1
6. Cundall, P. A., & Strack, O. D. L. (1979). A discrete numerical model for granular assemblies. *Géotechnique*, 29(1), 47–65. https://doi.org/10.1680/geot.1979.29.1.47
7. da Cruz, F., Emam, S., Prochnow, M., Roux, J.-N., & Chevoir, F. (2005). Rheophysics of dense granular materials: Discrete simulation of plane shear flows. *Physical Review E*, 72(2), 021309. https://doi.org/10.1103/PhysRevE.72.021309
8. Dagum, L., & Menon, R. (1998). OpenMP: An industry standard API for shared-memory programming. *IEEE Computational Science and Engineering*, 5(1), 46–55. https://doi.org/10.1109/99.660313
9. Dent, J. D., Burrell, K. J., Schmidt, D. S., Louge, M. Y., Adams, E. E., & Jazbutis, T. G. (1998). Density, velocity and friction measurements in a dry-snow avalanche. *Annals of Glaciology*, 26, 247–252. https://doi.org/10.3189/1998AoG26-1-247-252
10. Di Toro, G., Goldsby, D. L., & Tullis, T. E. (2004). Friction falls towards zero in quartz rock as slip velocity approaches seismic rates. *Nature*, 427(6973), 436–439. https://doi.org/10.1038/nature02249
11. Di Toro, G., Han, R., Hirose, T., De Paola, N., Nielsen, S., Mizoguchi, K., Ferri, F., Cocco, M., & Shimamoto, T. (2011). Fault lubrication during earthquakes. *Nature*, 471(7339), 494–498. https://doi.org/10.1038/nature09838
12. Elbanna, A. E., & Carlson, J. M. (2014). A two-scale model for sheared fault gouge: Competition between macroscopic disorder and local viscoplasticity. *Journal of Geophysical Research: Solid Earth*, 119(6), 4841–4859. https://doi.org/10.1002/2014JB011001
13. Ergenzinger, C., Seifried, R., & Eberhard, P. (2011). A discrete element model to describe failure of strong rock in uniaxial compression. *Granular Matter*, 4(13), 341–364. https://doi.org/10.1007/s10035-010-0230-7
14. Falk, M. L., & Langer, J. S. (1998). Dynamics of viscoplastic deformation in amorphous solids. *Physical Review E*, *57*(6), 7192–7205. https://doi.org/10.1103/PhysRevE.57.7192
15. Falk, M. L., & Langer, J. S. (2011). Deformation and failure of amorphous, solidlike materials. *Annual Review of Condensed Matter Physics*, 2(1), 353–373. https://doi.org/10.1146/annurev-conmatphys-062910-140452
16. Fraige, F. Y., & Langston, P. A. (2004). Integration schemes and damping algorithms in distinct element models. *Advanced Powder Technology*, 15(2), 227–245. https://doi.org/10.1163/156855204773644454
17. GDR MiDi. (2004). On dense granular flows. *The European Physical Journal. E, Soft Matter*, 14(4), 341–365. https://doi.org/10.1140/epje/i2003-10153-0
18. Goldsby, D. L., & Tullis, T. E. (2002). Low frictional strength of quartz rocks at subseismic slip rates. *Geophysical Research Letters*, 29(17). https://doi.org/10.1029/2002GL015240
19. Hirose, T., & Shimamoto, T. (2005). Growth of molten zone as a mechanism of slip weakening of simulated faults in gabbro during frictional melting. *Journal of Geophysical Research: Solid Earth*, 110(B5), 2004JB003207. https://doi.org/10.1029/2004JB003207

20. Ikari, M. J., Carpenter, B. M., Scuderi, M. M., Collettini, C., & Kopf, A. J. (2020). Frictional strengthening explored during non-steady state shearing: Implications for fault stability and slip event recurrence time. *Journal of Geophysical Research: Solid Earth*, 125(10), e2020JB020015. https://doi.org/10.1029/2020JB020015
21. Jop, P., Forterre, Y., & Pouliquen, O. (2006). A constitutive law for dense granular flows. *Nature*, 441(7094), 727–730. https://doi.org/10.1038/nature04801
22. Jutzi, M., & Asphaug, E. (2011). Forming the lunar farside highlands by accretion of a companion moon. *Nature*, 476(7358), 69–72. https://doi.org/10.1038/nature10289
23. Kitajima, H., Chester, F. M., & Chester, J. S. (2011). Dynamic weakening of gouge layers in high-speed shear experiments: Assessment of temperature-dependent friction, thermal pressurization, and flash heating. *Journal of Geophysical Research*, 116(B8), B08309. https://doi.org/10.1029/2010JB007879
24. Kitajima, H., Chester, J. S., Chester, F. M., & Shimamoto, T. (2010). High-speed friction of disaggregated ultracataclasite in rotary shear: Characterization of frictional heating, mechanical behavior, and microstructure evolution. *Journal of Geophysical Research (Solid Earth)*, 115, B08408. https://doi.org/10.1029/2009JB007038
25. Kothari, K. R., & Elbanna, A. E. (2017). Localization and instability in sheared granular materials: Role of friction and vibration. *Physical Review E*, 95(2), 022901. https://doi.org/10.1103/PhysRevE.95.022901
26. Lachenbruch, A. H. (1980). Frictional heating, fluid pressure, and the resistance to fault motion. *Journal of Geophysical Research*, *85*, 6097–6112. https://doi.org/10.1029/JB085iB11p06097
27. Langston, P. A., Tüzün, U., & Heyes, D. M. (1995). Discrete element simulation of granular flow in 2D and 3D hoppers: Dependence of discharge rate and wall stress on particle interactions. *Chemical Engineering Science*, 50, 967–987. https://doi.org/10.1016/0009-2509(94)00467-6
28. Lucas, A., Mangeney, A., & Ampuero, J. P. (2014). Frictional velocity-weakening in landslides on Earth and on other planetary bodies. *Nature Communications*, 5(1), 3417. https://doi.org/10.1038/ncomms4417
29. Ma, X., & Elbanna, A. (2018). Strain localization in dry sheared granular materials: A compactivity-based approach. *Physical Review E*, 98(2), 022906. https://doi.org/10.1103/PhysRevE.98.022906
30. Manning, M. L., & Liu, A. J. (2011). Vibrational modes identify soft spots in a sheared disordered packing. *Physical Review Letters*, 107(10), 108302. https://doi.org/10.1103/PhysRevLett.107.108302
31. Marone, C. (1998). Laboratory-derived friction laws and their application to seismic faulting. *Annual Review of Earth and Planetary Sciences*, 26, 643–696. https://doi.org/10.1146/annurev.earth.26.1.643
32. Mase, C. W., & Smith, L. (1987). Effects of frictional heating on the thermal, hydrologic, and mechanical response of a fault. *Journal of Geophysical Research: Solid Earth*, 92(B7), 6249–6272. https://doi.org/10.1029/JB092iB07p06249
33. Mollon, G., Aubry, J., & Schubnel, A. (2021). Simulating melting in 2d seismic fault gouge. *Journal of Geophysical Research: Solid Earth*, 126(6), e2020JB021485. https://doi.org/10.1029/2020JB021485
34. Morgan, J. K. (1999). Numerical simulations of granular shear zones using the distinct element method: 2. Effects of particle size distribution and interparticle friction on mechanical behavior. *Journal of Geophysical Research*, 104, 2721–2732. https://doi.org/10.1029/1998JB900055
35. Nielsen, S. (2017). From slow to fast faulting: Recent challenges in earthquake fault mechanics. *Philosophical Transactions. Series A, Mathematical, Physical, and Engineering Sciences*, *375(2*103), 20160016. https://doi.org/10.1098/rsta.2016.0016
36. O'Hara, K., Mizoguchi, K., Shimamoto, T., & Hower, J. C. (2006). Experimental frictional heating of coal gouge at seismic slip rates: Evidence for devolatilization and thermal pressurization of gouge fluids. Tectonophysics, 424(1), 109–118. https://doi.org/10.1016/j.tecto.2006.07.007
37. Papachristos, E., Stefanou, I., & Sulem, J. (2023). A discrete elements study of the frictional behavior of fault gouges. *Journal of Geophysical Research: Solid Earth*, 128(1), e2022JB025209. https://doi.org/10.1029/2022JB025209
38. Piroozan, N., & Sahimi, M. (2020). Molecular origin of sliding friction and flash heating in rock and heterogeneous materials. *Scientific Reports*, 10(1), 22264. https://doi.org/10.1038/s41598-020-79383-y
39. Potyondy, D. O., & Cundall, P. A. (2004). A bonded-particle model for rock. *International Journal of Rock Mechanics and Mining Sciences*, 41(8), 1329–1364. https://doi.org/10.1016/j.ijrmms.2004.09.011
40. Rice, J. R. (2006). Heating and weakening of faults during earthquake slip. *Journal of Geophysical Research: Solid Earth*, 111(B5), 2005JB004006. https://doi.org/10.1029/2005JB004006
41. Rice, J. R. (2017). Heating, weakening and shear localization in earthquake rupture. *Philosophical Transactions of the Royal Society A: Mathematical, Physical and Engineering Sciences*, 375(2103), 20160015. https://doi.org/10.1098/rsta.2016.0015
42. Sammis, C., King, G., & Biegel, R. (1987). The kinematics of gouge deformation. *Pure and Applied Geophysics*, 125, 777–812. https://doi.org/10.1007/BF00878033

43. Smeraglia, L., Billi, A., Carminati, E., Cavallo, A., Di Toro, G., Spagnuolo, E., & Zorzi, F. (2017). Ultra-thin clay layers facilitate seismic slip in carbonate faults. *Scientific Reports*, *7(1)*, 664. https://doi.org/10.1038/s41598-017-00717-4
44. Sone, H., & Shimamoto, T. (2009). Frictional resistance of faults during accelerating and decelerating earthquake slip. *Nature Geoscience*, 2, 705–708. https://doi.org/10.1038/ngeo637
45. Spagnuolo, E., Plümper, O., Violay, M., Cavallo, A., & Di Toro, G. (2015). Fast-moving dislocations trigger flash weakening in carbonate-bearing faults during earthquakes. *Scientific Reports*, 5, 16112. https://doi.org/10.1038/srep16112
46. Taboada, S., Renouf, M. (2023). Rheology and breakdown energy of a shear zone undergoing flash heating in earthquake-like discrete element models. *Geophysical Journal International*, 233 (2), pp.1492-1514. https://dx.doi.org/10.1093/gji/ggad004
47. Wibberley, C. A. J., & Shimamoto, T. (2005). Earthquake slip weakening and asperities explained by thermal pressurization. Nature, 436(7051), 689–692. https://doi.org/10.1038/nature03901
48. Wong, T., & Baud, P. (2012). The brittle-ductile transition in porous rock: A review. *Journal of Structural Geology*, 44, 25–53. https://doi.org/10.1016/j.jsg.2012.07.010